Transmission-type reconfigurable metasurface for linear-to-circular and linear-to-linear polarization conversions

Ping Wang(王平), Yu Wang(王豫), Zhongming Yan(严仲明)†, and Hongcheng Zhou(周洪澄)

School of Electrical Engineering, Southwest Jiaotong University, Chengdu 611756, *China*

(Received 25 May 2022; revised manuscript received 6 August 2022; accepted manuscript online 26 August 2022)

We present a transmission-type polarization conversion metamaterial (PCM) whose functions can be dynamically switched among the linear-to-circular (LTC) and linear-to-linear (LTL) polarization conversions. The proposed PCM consists of a grating, a polarization conversion surface and a reconfigurable polarization selective surface incorporated with PIN diodes. By changing the states of diodes, the PCM can achieve the reconfigurable manipulations for incident waves. The Fabry–Pérot (F–P) resonances excited by the PCM contribute to the polarization conversions, as is illustrated. Moreover, through establishing the F–P-like cavity model and analyzing the electric field components of the transmitted waves, the conditions for realizing LTC polarization conversion are revealed, which can guide the construction of PCM. The prototype of PCM is fabricated and measured, which can achieve LTC and LTL polarization conversions within 3.31–3.56 GHz and 2.76–4.24 GHz, respectively, the polarization conversion ratios of two functions are higher than 0.95. The measurement results are in agreement with the simulation data.

Keywords: polarization conversion, reconfigurable metasurface, Fabry–Pérot resonance

PACS: 42.25.Bs, 42.25.Ja, 81.05.Xj **DOI:** 10.1088/1674-1056/ac8ce0

1. Introduction

Polarization is one of the fundamental properties of electromagnetic (EM) waves, which carries plenty of information about the scatters. Thus, the polarization modulation is significant and valuable in many aspects, such as wireless communication,[1–3] radar cross section reduction,[4,5] and imaging.[6,7] To process polarization information as much as possible, the devices which can manipulate multiple polarization are essential. Metasurfaces have provided excellent alternatives. As a two-dimensional artificial material, metasurfaces have been widely utilized to control EM waves because of their low profile, low loss, easy processing, high flexibility, and so on. For possessing tunable property and functionality, various reconfigurable metasurfaces were fabricated by integrating with RF devices[8–16] or functional materials.[17,18]

It has always been pursued to manipulate the polarization of waves at will. To date, various reconfigurable polarization conversion metasurfaces (PCMs) with multiple functions have been proposed. However, the major of reported transmission-type PCM can only achieve co-polarization transmission and a single polarization conversion. For example, the reconfigurable PCMs composed of periodic rings[8] or chiral structures[9] incorporated with PIN diodes were proposed, which can realize co-polarization transmission and linear-to-circular (LTC) polarization conversion. Some reconfigurable PCMs formed by split rings achieved co-polarization transmission and linear-to-linear (LTL) polarization conversion.[10,11] However, the dynamic switching among LTC and LTL polarization conversions is still rare for the transmission-type PCM. In Ref. [16], the bi-layer PCM incorporated with varactor diodes was proposed, it could convert the incident LP waves into multiple polarization, but it could only operate in narrow frequency band. The integration of LTC and LTL polarization conversions has been concerned.[19–21] To solve the problem, several designs based on passive metasurfaces were reported. Unfortunately, their operational bands for each function cannot overlap, which causes the reported designs impossible to process multi-polarization signals with the same frequency. The design proposed in Refs. [22,23] can reconfigure the incident linear polarization to multiple linear and circular polarization by rotating the metasurfaces, but the slow mechanical adjustment may be limited in applications.

In this paper, we design a novel transmission-type reconfigurable PCM based on Fabry–Pérot (F–P) resonate cavity for LTC and LTL polarization conversions. The proposed PCM consists of a layer of grating, a polarization conversion surface and a reconfigurable polarization selective surface. The switching of functions is realized by changing states of the PIN diodes. To verify the design, the prototype has been fabricated and tested. As demonstrated by the measurement results, the PCM can convert linear polarized (LP) waves to CP waves from 3.31 GHz to 3.56 GHz with the axial ratio (AR) less than 3 dB when the PIN diodes are switched off. Instead, when the diodes are switched on, the PCM can rotate the LP waves to cross-polarized waves from 2.76 GHz to 4.24 GHz with the polarization conversion ratio (PCR) higher than 0.95. The operational bandwidths are 7.3% and 42.3% for the LTC and LTL polarization conversions. The thickness of proposed PCM is $0.2\lambda_0$ (λ_0 is the wavelength corresponding to the central frequency). Moreover, the F–P resonance excited in the

†Corresponding author. E-mail: yzm@swjtu.edu.cn

© 2022 Chinese Physical Society and IOP Publishing Ltd

PCM is discussed in this paper, and the conditions for realizing LTC polarization conversion are also derived. Before our work, a lot of LTL polarization converters combining F–P resonate cavity have been proposed.[24–26] Nevertheless, to the best of our knowledge, the transmission-type LTC polarization converter based on F–P cavity-like metasurface has not been reported. Our proposed design provides a new method for converting incident linear polarized wave into circular polarized and cross-polarized wave, which may promote the development of transmission-type metasurface toward arbitrary polarization manipulations.

2. Analysis and design

2.1. Operational principles of the PCM

For achieving dynamically switching among LTC and LTL polarization conversions, we propose an approach for constructing the PCM whose schematic diagram is depicted in Fig. 1. Layer A is a polarization selector which only permits the y-polarized wave to pass through. Layer B is a polarization conversion surface composed of periodic anisotropic structures, which can partially converts the incident y-polarized wave into x polarization. The reconfigurable layer C which integrates PIN diodes has two functions, including co-polarization transmission and polarization selection. The three layers form an F–P resonate cavity. The corresponding relationships between the states of PIN diodes and the PCM are illustrated in Table 1.

Table 1. Working states of PIN diodes and functions of PCM.

	PIN diode	Layer C	PCM
State 1	off	x-polarized transmission y-polarized transmission	LTC polarization conversion
State 2	on	x-polarized transmission y-polarized reflection	LTL polarization conversion

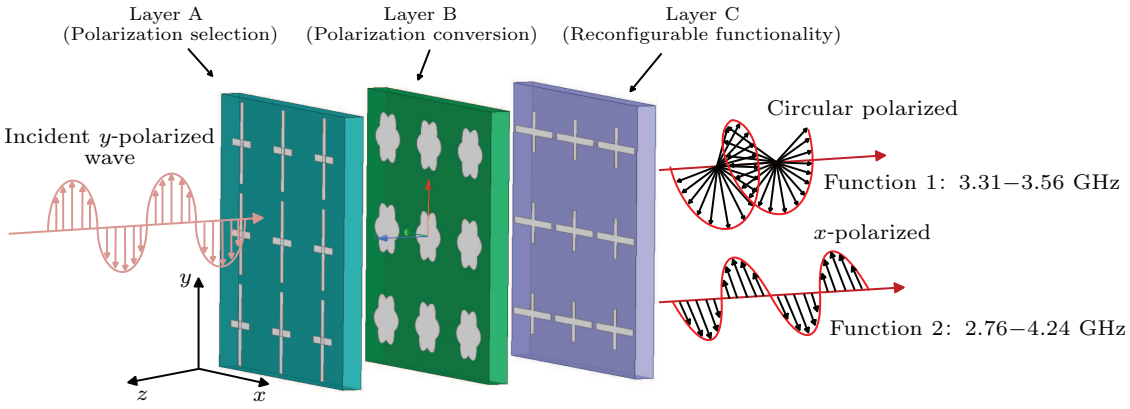


Fig. 1. Schematic diagram of proposed PCM for polarization conversion.

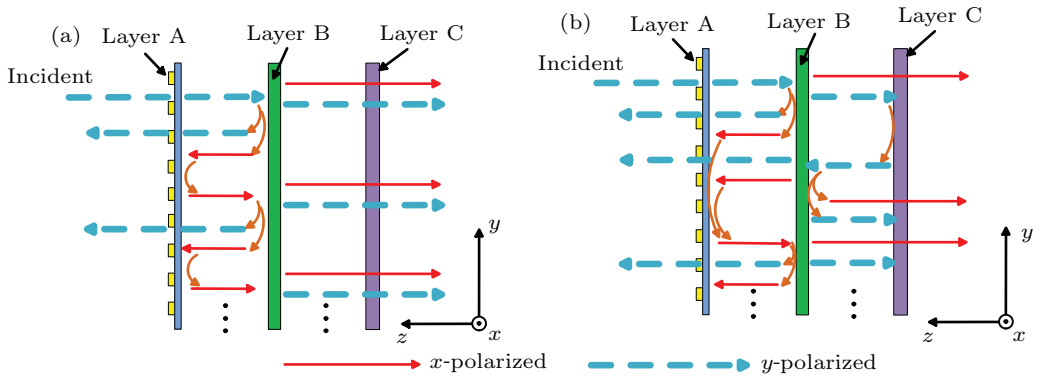


Fig. 2. The schematic diagram of the propagation of waves in PCM, as the state of PIN diode is switched (a) off and (b) on.

For describing the operational principle, we have established an F–P resonate model based on the PCM as shown in Fig. 2. The y-polarized waves illuminate PCM along $-z$ axis, and the transmission directions of waves in PCM are indicated by the arrows. The y- and x-polarized components are denoted by solid and dashed lines, respectively. First, the incident y-polarized waves pass through layer A and interact with layer B, then the reflected and transmitted waves which include y- and x-polarized components are excited by layer B. The y-polarized backward wave penetrates into layer A, the x-polarized one is reflected by layer A and interacts with layer B once again. In contrast, the propagation processes of forward waves depend on states of layer C. If layer C is in state 1, as shown in Fig. 2(a), the y- and x-polarized components

can pass through it. When layer C is in state 2, as shown in Fig. 2(b), only the x-polarized component can pass through it. The y-polarized component will be reflected by layer C and undergoes the multiple reflections. It should be noted that the above descriptions of wave propagation in state 1 ignore the reflection of layer C, in fact, a few of y- and x-polarized components will be reflected by it and participate in the round trips within the PCM.

Based on the analysis of the interactions between waves and metasurface (see Appendix for details), we derived the condition for the PCM achieving LTC polarization conversion as follows:

$$\frac{t^{\mathrm{B}}_{uu}}{t^{\mathrm{B}}_{vv}} = \mathrm{e}^{\pm j\frac{\pi}{2}} \cdot \frac{1 + r^{\mathrm{B}}_{uu} \cdot \mathrm{e}^{\mathrm{j}2k_0 d_0} + r^{\mathrm{C}} \cdot \mathrm{e}^{\mathrm{j}2k_0 d_1} \cdot \{[(t^{\mathrm{B}}_{uu})^2 - (r^{\mathrm{B}}_{uu})^2] \cdot \mathrm{e}^{\mathrm{j}2k_0 d_0} - r^{\mathrm{B}}_{uu}\}}{1 + r^{\mathrm{B}}_{vv} \cdot \mathrm{e}^{\mathrm{j}2k_0 d_0} + r^{\mathrm{C}} \cdot \mathrm{e}^{\mathrm{j}2k_0 d_1} \cdot \{[(t^{\mathrm{B}}_{vv})^2 - (r^{\mathrm{B}}_{vv})^2] \cdot \mathrm{e}^{\mathrm{j}2k_0 d_0} - r^{\mathrm{B}}_{vv}\}}, \tag{1}$$

where $t^m_{\alpha\beta}$ ($r^m_{\alpha\beta}$) denotes the transmission (reflection) coefficients of the β-polarized incident wave converted into a α-polarized wave, the superscripts m denotes different layers. The k is the free-space wave number. Moreover, Eq. (1) takes into account the reflection on layer C. The x–y and u–v coordinate systems are shown in Fig. 3. It should be noted that Eq. (1) is valid for layer B with a specific category of structure, whose responses at u- and v-directions are independent of each other, i.e., $t_{uv} = t_{vu} = r_{uv} = r_{vu} = 0$. The fabrication of layer B can utilize the cross-shaped elements similar to structures proposed in Refs. [27,28]. If the reflection of layer C is very low, the condition can be simplified to

$$\frac{t^{\mathrm{B}}_{uu}}{t^{\mathrm{B}}_{vv}} = \mathrm{e}^{\pm \mathrm{j}\frac{\pi}{2}} \cdot \frac{1 + r^{\mathrm{B}}_{uu} \cdot \mathrm{e}^{\mathrm{j}2k_0 d_0}}{1 + r^{\mathrm{B}}_{vv} \cdot \mathrm{e}^{\mathrm{j}2k_0 d_0}}. \tag{2}$$

To realize LTC polarization conversion, the strategy we adopted is to determine the geometric parameters which can affect the t^{B}_{uu} and r^{B}_{uu} first, then to adjust the parameters related to t^{B}_{vv} and r^{B}_{vv}, and finally to modulate the distances between adjacent layers until the condition is met.

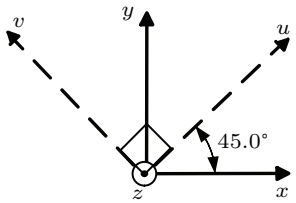


Fig. 3. Schematic diagram of the x–y and u–v coordinate systems.

2.2. Design of geometric configuration for each layer

The unit cells of layer A and B are shown in Fig. 4. The dielectric substrates are FR4 with relative permittivity $\varepsilon_r = 4.3$. Several metal stripes along x-axis are etched on front side of layer A, which form a grating. For filtering out the x-polarized incident waves, the geometry parameters of layer A are chosen as $w_1 = 2.5$ mm, $g_1 = 3.5$ mm, the thickness of substrate in layer A is $t_1 = 0.5$ mm. The metal stripes and successive lines are orthogonal, they are etched on the front side of layer B. The thickness of substrate in layer B is $t_2 = 1.6$ mm.

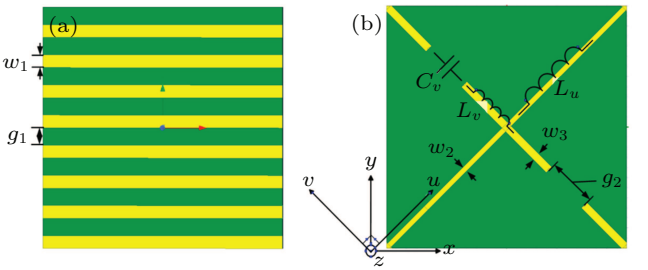


Fig. 4. The geometric configuration of unit cell: (a) layer A, (b) layer B.

The equivalent circuits of layer B at u- and v-polarization are illustrated in Fig. 5, where L_u and L_v denote the inductance introduced by the metal strips along u- and v-axis, C_v denotes the capacitance of the gap between two strips aligned with v-axis. Z_{sub} represents the equivalent impedance of the substrate. The $ABCD$ matrix of layer B can be expressed as[29]

$$\begin{bmatrix} A & B \\ C & D \end{bmatrix} = \boldsymbol{M}_{\mathrm{p}} \cdot \boldsymbol{M}_{\mathrm{s}}, \tag{3}$$

$$\boldsymbol{M}_{\mathrm{p}} = \begin{bmatrix} 1 & 0 \\ 1/Z_i & 1 \end{bmatrix}, \tag{4}$$

$$\boldsymbol{M}_{\mathrm{p}} = \begin{bmatrix} \cos(k_0\sqrt{\varepsilon_{\mathrm{r}}} \cdot t_2) & \mathrm{j} \cdot Z_0 \sin(k_0\sqrt{\varepsilon_{\mathrm{r}}} \cdot t_2)/\sqrt{\varepsilon_{\mathrm{r}}} \\ \mathrm{j}\sqrt{\varepsilon_{\mathrm{r}}} \sin(k_0\sqrt{\varepsilon_{\mathrm{r}}} \cdot t_2)/Z_0 & \cos(k_0\sqrt{\varepsilon_{\mathrm{r}}} \cdot t_2) \end{bmatrix}, \tag{5}$$

where $\boldsymbol{M}_{\mathrm{p}}$ and $\boldsymbol{M}_{\mathrm{s}}$ represent the transmission matrix of metal patterns and substrate of layer B. Z_i denotes the impedance of metal patterns with $i = u$ or $i = v$ depending on the polarization direction. The impedance can be derived as $Z_u = \mathrm{j}\omega L_u$ and $Z_v = \mathrm{j}(2\omega L_v - 2/\omega C_v)$. The circuit parameters can be obtained as follows:[14,30]

$$L_u = \frac{\sqrt{2}\mu_0 p}{2\pi} \ln\left(\frac{2\sqrt{2}p}{\pi w_2}\right), \tag{6}$$

$$L_v = \frac{\sqrt{2}\mu_0 p}{4\pi} \ln[1/\sin(\sqrt{2}\pi w_3/2p)], \tag{7}$$

$$C_v = \frac{\varepsilon_0 p\sqrt{\varepsilon_{\mathrm{r}}+1}}{\pi} \ln[1/\sin(\sqrt{2}\pi g_2/2p)]. \tag{8}$$

Then, the co-polarized transmission and reflection coefficients of layer B can be calculated by

$$t^{\mathrm{B}} = \frac{2}{A+B/Z_0+CZ_0+D}, \tag{9}$$

$$r^{\mathrm{B}} = \frac{A+B/Z_0-CZ_0-D}{A+B/Z_0+CZ_0+D}. \tag{10}$$

Via adjusting the w_2 and g_2, the co-polarization transmission and reflection coefficients aligned with u- and v-axis can be independently tuned. The value selections of w_2 and g_2 according to performance of layer B will be described in the following section.

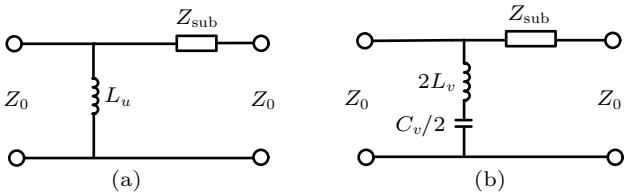


Fig. 5. The equivalent circuit model of layer B. The incident wave is (a) u-polarized (b) v-polarized.

The periodic structure of layer C is presented in Figs. 6(a) and 6(b), the rectangular metal patches are arranged on the front side. The PIN diodes are embedded into the gaps between adjacent patches. The orthogonal metal lines are etched on the back side of layer C. The PIN diode is Skyworks SMP1345-079LF. For the on state, it can be equivalent to a resistor of 2 Ω in series with an inductor of 0.7 nH. For the off state, it can be equivalent to a capacitor of 0.15 pF in series with an inductor of 0.7 nH. The dielectric substrate employed in layer C is same as in layer B. The geometric parameters of layer C are taken as $l_2 = 5.13$ mm, $g_3 = 2.19$ mm, $w_4 = 3.14$ mm, $w_5 = 0.5$ mm, $w_6 = 0.8$ mm, $w_7 = 0.4$ mm, and $p_1 = 16$ mm. For describing the operational principle of layer C, the lumped circuit elements introduced by the metal patterns are illustrating in Fig. 6(a). Here L_1 and L_3 denote the equivalent inductance of the metal patch at y and x directions, respectively, C_1 is the capacitor introduced by the gap between patches along x-axis. The inductances of metal wires on back side are denoted by L_2 and L_4, respectively. When the PIN diodes are switched off, the front-side structures exhibit capacitive responses along x and y directions, after cascading with the inductive branches on the backside, layer C will exhibit band-pass response for incident waves. While the PIN diodes are switched on, layer C can be equivalent to a metal grating parallel to y-axis for blocking the y-polarized waves. The simulated results of layer C are shown in Fig. 6(c). With the changing of PIN states, there is obvious discrepancy for the transmission of y-polarized wave. For the off state, the $|t_{yy}|$ is consistent with $|t_{xx}|$, which are higher than −1 dB within 2.42–3.80 GHz, for the on state, the $|t_{yy}|$ is less than −20.3 dB below 3.80 GHz.

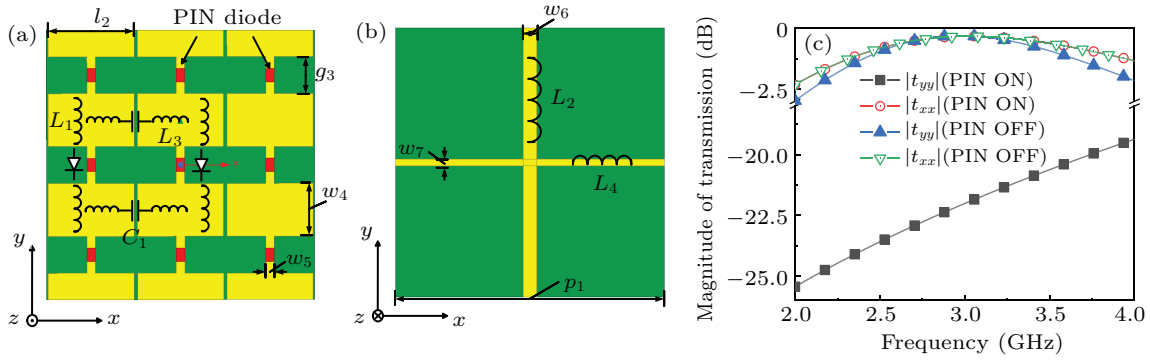


Fig. 6. The geometric configuration of periodic structures in layer C: (a) front side, (b) back side. (c) Simulated transmission coefficients of layer C.

2.3. Integrated design of the PCM

By cascading the proposed three layers, as shown in Fig. 7, the PCM is constructed. Then, several geometric parameters need to be determined according to performance of the PCM, including the configuration of the layer B and the distances between adjacent layers. The optimization target for the PCM is to realize LTC and LTL polarization conversions within S-band, and the performances of LTC conversion are set as priority. Based on Eq. (1) and related discussions, the optimizations can follow the principles mentioned below. First, the periodic dimension p and line width w_2 should be determined, which mainly depend on the predetermined transmittance and operational frequency. The increase of p and the decrease of w_2 are conducive to improve the transmittance t^{B}_{uu} because the equivalent inductances of successive metal lines are raised. However, p should not exceed half a wavelength in order to suppress the gating lobes.[30] Next, we can optimize the performances of LTC conversion by adjusting g_2 and d. The frequency responses of the AR with different g_2 and d are shown in Fig. 8 with $p = 48$ mm and $w_2 = 0.1$ mm. The AR of PCM is obtained as follows:

$$\mathrm{AR}=\left(\frac{\left|t_{xy}^{\mathrm{I+II}}\right|^2+\left|t_{yy}^{\mathrm{I+II}}\right|^2+\sqrt{a}}{\left|t_{xy}^{\mathrm{I+II}}\right|^2+\left|t_{yy}^{\mathrm{I+II}}\right|^2-\sqrt{a}}\right)^{\frac{1}{2}}, \tag{11}$$

$$a=\left|t_{xy}^{\mathrm{I+II}}\right|^4+\left|t_{yy}^{\mathrm{I+II}}\right|^4+2\left|t_{xy}^{\mathrm{I+II}}\right|^2\left|t_{yy}^{\mathrm{I+II}}\right|^2\cos(2\Delta\varphi_{xy}). \tag{12}$$

It can be found that the minimal value of AR is mainly determined by g_2, and the operational frequency is mainly determined by d. We can select the value of g_2 first to guarantee the LTC polarization conversion, and then optimize the overlapping bandwidth and conversion coefficients of LTC and LTL polarization conversions by adjusting d. Finally, the performances of PCM can be finely tuned by adjusting d_1. The optimized geometric parameters are taken as $p=48$ mm, $w_2=1.5$ mm, $g_2=9$ mm, $d=7$ mm, $d_1=7$ mm.

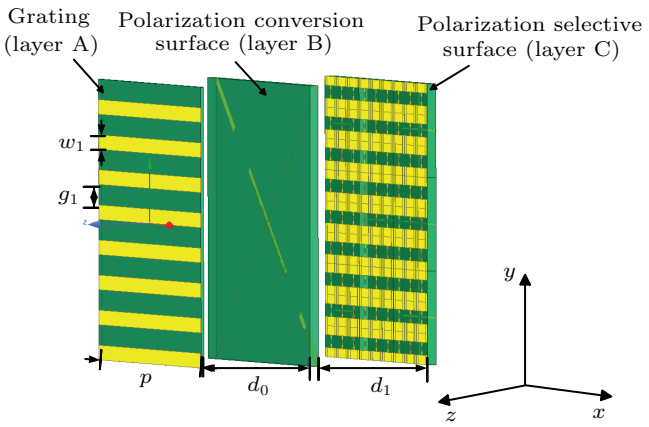


Fig. 7. Configuration of unit cell of the proposed PCM.

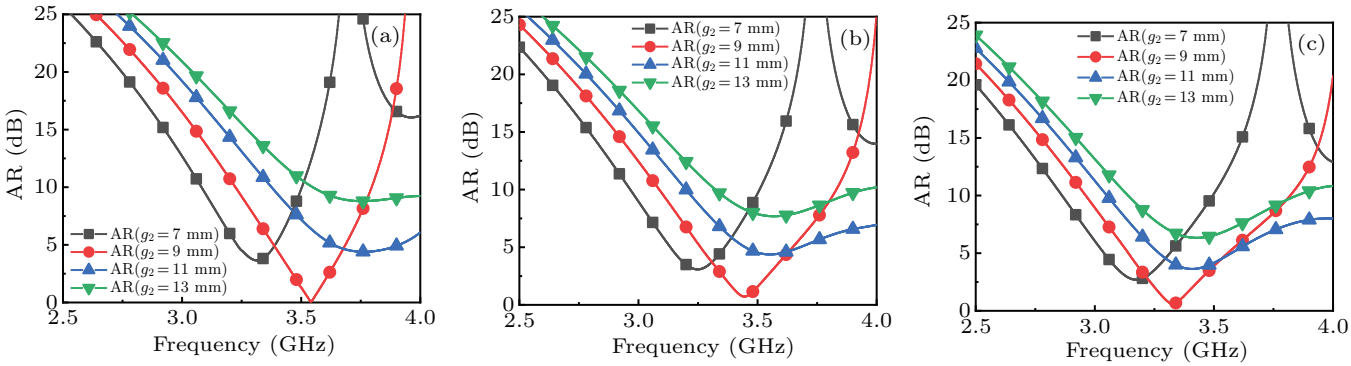


Fig. 8. The comparison of AR with different g_2 and d: (a) $d=5$ mm, (b) $d=7$ mm, (c) $d=9$ mm.

3. Simulation and measurement results

The model of proposed PCM is simulated by the CST Microwave Studio, and the prototype of PCM is fabricated and measured. The experimental setups are illustrated in Fig. 9, two horn antennas are placed on different sides of prototype, which are connected to the Keysight N5227B vector network analyzer (VNA) through RF cables. The size of prototype is 330 mm×330 mm×17.7 mm, and the thickness is $0.2\lambda_0$ (λ_0 is wavelength corresponding to the central frequency). The simulation and measurement results are shown in Fig. 10, where t_{-y} and t_{+y} denote the transmission from y-polarized to lift-handed and right-handed circular polarizations, respectively. They can be obtained as follows:

$$t_{-y}=\frac{\sqrt{2}}{2}(t_{xy}+\mathrm{j}\cdot t_{yy}), \tag{13}$$

$$t_{+y}=\frac{\sqrt{2}}{2}(t_{xy}-\mathrm{j}\cdot t_{yy}). \tag{14}$$

The PCR at LTC and LTL mode is defined as $|t_{-y}|^2/(|t_{-y}|^2+|t_{+y}|^2)$ and $|t_{xy}|^2/(|t_{xy}|^2+|t_{yy}|^2)$.[10,30] As shown in the measurement results, when the PIN diodes are switched off, the PCM can achieve LTC polarization conversion with the AR less than 3 dB from 3.31 GHz to 3.56 GHz. Meanwhile, the PCR of LTC polarization conversion is higher than 0.95.

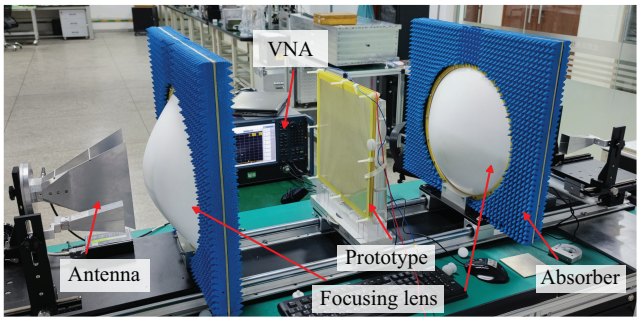


Fig. 9. The measurement setup and prototype.

When the PIN diodes are switched on, the PCM can rotate y-polarized wave to x-polarization with the PCR higher than 0.95 within 2.76–4.24 GHz. The fractional bandwidths at LTC and LTL modes are 7.3% and 42.3%, respectively. In the overlapping frequency band, the magnitudes of transmissions of both functions are higher than −1.84 dB. In Fig. 10, the measurement results show agreement with the simulation ones, there are some discrepancies which may be caused by the deviations in fabrication of prototype and instrument alignment. Moreover, we obtain the analytic transmission coefficients of PCM according to the discussions in Appendix, which are basically consistent with the simulation and measurement results. Even if there are deviations, the comparison in Fig. 10 indicates that the proposed expressions in Appendix

can effectively represent the transmission coefficient of PCM. In Appendix, it is assumed that the magnitude of transmittance of layer A to y-polarized wave (the same as the magnitude of reflectivity to x-polarized wave) is 1, whereas the transmittance of layer A in fact will be slightly smaller, which may cause the deviations of the analytic results.

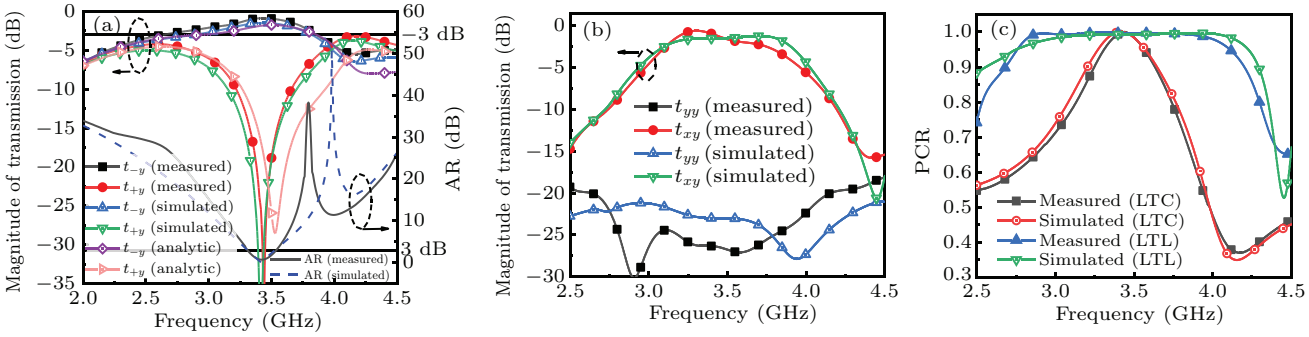


Fig. 10. The measurement and simulation results of the PCM: (a) magnitude of transmission and AR for LTC polarization conversion, (b) magnitude of transmission for LTL polarization conversion, (c) PCR for LTC and LTL polarization conversions.

The transmission coefficients of layer B are shown in Fig. 11, where the shadow area indicates the operational frequency band of LTC polarization conversion. It can be found that the magnitude of t_{vv}^{B} rapidly declines with frequency increasing in the operational band. Although the condition of polarization conversion can be satisfied near 3.43 GHz, the sharp change of parameters will limit the functionality to a narrow band. If a metasurface with stable response against frequency is used as layer B, the frequency band will be expanded, such as the multi-resonant structures[31] and multi-layer surface,[32] while the profile or insertion loss may be higher than the proposed design. Moreover, if the proposed layer B is replaced by a reconfigurable metasurface with appropriate configuration, the PCM may integrate more functions, such as co-polarized transmission and linear-to-elliptical polarization conversions.

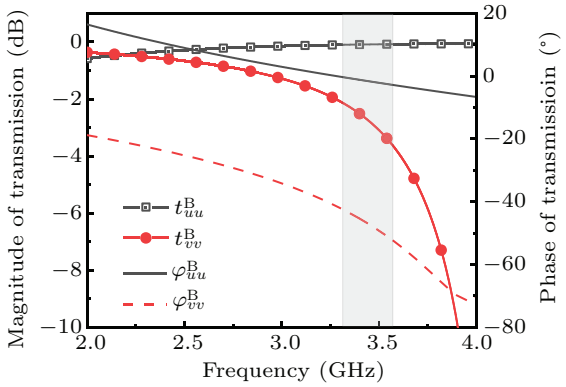


Fig. 11. The simulated magnitude and phase of transmission for layer B.

4. Conclusion

In summary, we have proposed a transmission-type reconfigurable PCM as well as detailed procedure, which has the reconfigurable functions of LTC and LTL polarization conversions. The reconfigurable functions are obtained by changing the states of PIN diodes embedded on the PCM. The operation of PCM is based on F–P resonances which have been illustrated. Moreover, to guide the design, the conditions for achieving LTC polarization conversion have been derived. From the measurement results of prototype, the overlapping frequency band of two functions is from 3.31 GHz to 3.56 GHz with the transmission higher than −1.84 dB. The thickness of the proposed PCM is $0.2\lambda_0$. Because the transmission-type metasurfaces can be loaded on aperture of the feeding antenna, the proposed design is more suitable for compact system than reflector arrays. It can also quickly switch states due to its electronic adjustment. These advantages make the proposed PCM have the application prospects in S-band radar and satellite communication, meanwhile it also has the potential to merge more functionalities of EM wave manipulation.

Appendix A

To analyze the propagation of incident waves in the PCM, we divide PCM into two parts at first. As shown in Fig. A1, layer A is named as part I, the layers B and C are regarded as a whole and indicated as part Ⅱ. The x- and y-polarized electric field components are denoted by $E_{xn}^{\mathrm{t/r}}$or $E_{yn}^{\mathrm{t/r}}$, where n in the subscript indicates the component experienced n times round-trips within the space between adjacent layers. We assume that the Jones matrixes describing layer A satisfy

$$\boldsymbol{T}=\begin{bmatrix} t_{yy}^{\mathrm{A}} & t_{yx}^{\mathrm{A}} \\ t_{xy}^{\mathrm{A}} & t_{xx}^{\mathrm{A}} \end{bmatrix}=\begin{bmatrix} 0 & 0 \\ 0 & 1 \end{bmatrix},$$
$$\boldsymbol{R}=\begin{bmatrix} r_{yy}^{\mathrm{A}} & r_{yx}^{\mathrm{A}} \\ r_{xy}^{\mathrm{A}} & r_{xx}^{\mathrm{A}} \end{bmatrix}=\begin{bmatrix} 1\cdot \mathrm{e}^{\mathrm{j}\pi} & 0 \\ 0 & 0 \end{bmatrix}. \tag{A1}$$

One can refer to the analysis in Ref. [21]. The total x- and y-polarized electric field components of the bi-layer structure in Fig. A1(a) can be expressed as

$$\boldsymbol{E}_y^{\mathrm{t}}=\boldsymbol{E}_y^{\mathrm{i}}\cdot t_{yy}^{\mathrm{I+II}}=\boldsymbol{E}_y^{\mathrm{i}}\cdot\left[t_{yy}^{\mathrm{II}}\cdot \mathrm{e}^{\mathrm{j}k_0d_0}-\frac{r_{xy}^{\mathrm{II}}\cdot t_{yx}^{\mathrm{II}}\cdot \mathrm{e}^{\mathrm{j}3k_0d_0}}{1+r_{xx}^{\mathrm{II}}\cdot \mathrm{e}^{\mathrm{j}2k_0d_0}}\right], \tag{A2}$$

$$\boldsymbol{E}_x^{\mathrm{t}} = \boldsymbol{E}_x^{\mathrm{i}} \cdot t_{xy}^{\mathrm{I+II}} = \boldsymbol{E}_x^{\mathrm{i}} \cdot \left[t_{xy}^{\mathrm{II}} \cdot \mathrm{e}^{\mathrm{j}k_0 d_0} - \frac{r_{xy}^{\mathrm{II}} \cdot t_{xx}^{\mathrm{II}} \cdot \mathrm{e}^{\mathrm{j}3k_0 d_0}}{1 + r_{xx}^{\mathrm{II}} \cdot \mathrm{e}^{\mathrm{j}2k_0 d_0}} \right]. \quad \text{(A3)}$$

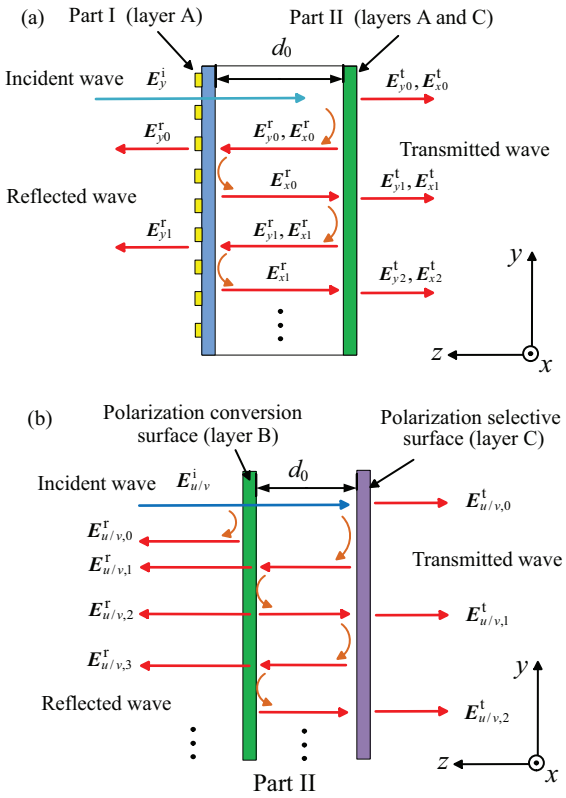


Fig. A1. The schematic diagram of the PCM with F–P resonance: (a) F–P resonance excited in the PCM, (b) F–P resonance excited in layer B and layer C.

In this paper, the near-field coupling excited between layers is not considered in the analysis of wave transmissions. Next, we present the propagation of waves in part Ⅱ. The schematic diagram is given in Fig. A1(b). For simplifying analysis, the transmission coefficients in the u–v coordinate system is discussed first. As mentioned above, the responses of layer B aligned with u and v axes are independent of each other. Therefore, u-polarized transmitted components can calculated as

$$\boldsymbol{E}_{u0}^{\mathrm{t}} = \boldsymbol{E}_u^{\mathrm{i}} \cdot t_{uu}^{\mathrm{B}} \cdot t^{\mathrm{C}} \cdot \mathrm{e}^{\mathrm{j}k_0 d_1}, \quad \text{(A4)}$$

$$\boldsymbol{E}_{u1}^{\mathrm{t}} = \boldsymbol{E}_u^{\mathrm{i}} \cdot t_{uu}^{\mathrm{B}} \cdot r^{\mathrm{C}} \cdot r_{uu}^{\mathrm{B}} \cdot t^{\mathrm{C}} \cdot \mathrm{e}^{\mathrm{j}3k_0 d_1}, \quad \text{(A5)}$$

$$\boldsymbol{E}_{u2}^{\mathrm{t}} = \boldsymbol{E}_u^{\mathrm{i}} \cdot t_{uu}^{\mathrm{B}} \cdot (r^{\mathrm{C}})^2 \cdot (r_{uu}^{\mathrm{B}})^2 \cdot t^{\mathrm{C}} \cdot \mathrm{e}^{\mathrm{j}5k_0 d_1}, \quad \text{(A6)}$$

$$\vdots$$

$$\boldsymbol{E}_{un}^{\mathrm{t}} = \boldsymbol{E}_u^{\mathrm{i}} \cdot t_{uu}^{\mathrm{B}} \cdot (r^{\mathrm{C}})^n \cdot (r_{uu}^{\mathrm{B}})^n \cdot t^{\mathrm{C}} \cdot \mathrm{e}^{\mathrm{j}(2n+1)k_0 d_1}. \quad \text{(A7)}$$

The total u-polarized transmitted component can be obtain as

$$\boldsymbol{E}_u^{\mathrm{t}} = \boldsymbol{E}_u^{\mathrm{i}} \cdot t_{uu}^{\mathrm{II}} = \lim_{n\to\infty} \sum_{N=0}^{n} \boldsymbol{E}_{uN}^{\mathrm{t}} = \boldsymbol{E}_u^{\mathrm{i}} \cdot \frac{t_{uu}^{\mathrm{B}} \cdot t^{\mathrm{C}} \cdot \mathrm{e}^{\mathrm{j}k_0 d_1}}{1 - r_{uu}^{\mathrm{B}} \cdot r^{\mathrm{C}} \cdot \mathrm{e}^{\mathrm{j}2k_0 d_1}}. \quad \text{(A8)}$$

Similarly, the total u-polarized transmitted component is

$$\boldsymbol{E}_v^{\mathrm{t}} = \boldsymbol{E}_v^{\mathrm{i}} \cdot t_{vv}^{\mathrm{II}} = \lim_{n\to\infty} \sum_{N=0}^{n} \boldsymbol{E}_{vN}^{\mathrm{t}} = \boldsymbol{E}_v^{\mathrm{i}} \cdot \frac{t_{vv}^{\mathrm{B}} \cdot t^{\mathrm{C}} \cdot \mathrm{e}^{\mathrm{j}k_0 d_1}}{1 - r_{vv}^{\mathrm{B}} \cdot r^{\mathrm{C}} \cdot \mathrm{e}^{\mathrm{j}2k_0 d_1}}. \quad \text{(A9)}$$

The reflected components can be similarly calculated as follows:

$$\begin{aligned} \boldsymbol{E}_u^{\mathrm{r}} &= \boldsymbol{E}_u^{\mathrm{i}} \cdot r_{uu}^{\mathrm{II}} = \lim_{n\to\infty} \sum_{N=0}^{n} \boldsymbol{E}_{uN}^{\mathrm{r}} \\ &= \boldsymbol{E}_u^{\mathrm{i}} \cdot \left[r_{uu}^{\mathrm{B}} + \frac{(t_{uu}^{\mathrm{B}})^2 \cdot r^{\mathrm{C}} \cdot \mathrm{e}^{\mathrm{j}2k_0 d_1}}{1 - r^{\mathrm{C}} \cdot r_{uu}^{\mathrm{B}} \cdot \mathrm{e}^{\mathrm{j}2k_0 d_1}} \right], \end{aligned} \quad \text{(A10)}$$

$$\begin{aligned} \boldsymbol{E}_v^{\mathrm{r}} &= \boldsymbol{E}_v^{\mathrm{i}} \cdot r_{vv}^{\mathrm{II}} = \lim_{n\to\infty} \sum_{N=0}^{n} \boldsymbol{E}_{vN}^{\mathrm{r}} \\ &= \boldsymbol{E}_v^{\mathrm{i}} \cdot \left[r_{vv}^{\mathrm{B}} + \frac{(t_{vv}^{\mathrm{B}})^2 \cdot r^{\mathrm{C}} \cdot \mathrm{e}^{\mathrm{j}2k_0 d_1}}{1 - r^{\mathrm{C}} \cdot r_{vv}^{\mathrm{B}} \cdot \mathrm{e}^{\mathrm{j}2k_0 d_1}} \right]. \end{aligned} \quad \text{(A11)}$$

The transmission and reflection matrixes of part Ⅱ in the xy coordinate system can be calculated as

$$\begin{bmatrix} t_{yy}^{\mathrm{II}} & t_{yx}^{\mathrm{II}} \\ t_{xy}^{\mathrm{II}} & t_{xx}^{\mathrm{II}} \end{bmatrix} = \boldsymbol{Q} \cdot \begin{bmatrix} t_{vv}^{\mathrm{II}} & t_{vu}^{\mathrm{II}} \\ t_{uv}^{\mathrm{II}} & t_{uu}^{\mathrm{II}} \end{bmatrix} \cdot \boldsymbol{Q}^{-1}, \quad \text{(A12)}$$

$$\begin{bmatrix} r_{yy}^{\mathrm{II}} & r_{yx}^{\mathrm{II}} \\ r_{xy}^{\mathrm{II}} & r_{xx}^{\mathrm{II}} \end{bmatrix} = \boldsymbol{Q} \cdot \begin{bmatrix} r_{vv}^{\mathrm{II}} & r_{vu}^{\mathrm{II}} \\ r_{uv}^{\mathrm{II}} & r_{uu}^{\mathrm{II}} \end{bmatrix} \cdot \boldsymbol{Q}^{-1}, \quad \text{(A13)}$$

where $\boldsymbol{Q}$ is the rotation matrix

$$\boldsymbol{Q} = \begin{bmatrix} \frac{\sqrt{2}}{2} & -\frac{\sqrt{2}}{2} \\ \frac{\sqrt{2}}{2} & \frac{\sqrt{2}}{2} \end{bmatrix}. \quad \text{(A14)}$$

According to Eqs. (A2), (A3) and (A12)–(A14), we can obtain the transmission coefficients of PCM:

$$t_{yy}^{\mathrm{I+II}} = \frac{(t_{uu}^{\mathrm{II}} + t_{vv}^{\mathrm{II}}) \cdot \mathrm{e}^{\mathrm{j}k_0 d_0} + (t_{vv}^{\mathrm{II}} \cdot r_{uu}^{\mathrm{II}} + t_{uu}^{\mathrm{II}} \cdot r_{vv}^{\mathrm{II}}) \cdot \mathrm{e}^{\mathrm{j}3k_0 d_0}}{2 + (r_{uu}^{\mathrm{II}} + r_{vv}^{\mathrm{II}}) \cdot \mathrm{e}^{\mathrm{j}2k_0 d_0}}, \quad \text{(A15)}$$

$$t_{xy}^{\mathrm{I+II}} = \frac{(t_{vv}^{\mathrm{II}} - t_{uu}^{\mathrm{II}}) \cdot \mathrm{e}^{\mathrm{j}k_0 d_0} + (t_{vv}^{\mathrm{II}} \cdot r_{uu}^{\mathrm{II}} - t_{uu}^{\mathrm{II}} \cdot r_{vv}^{\mathrm{II}}) \cdot \mathrm{e}^{\mathrm{j}3k_0 d_0}}{2 + (r_{uu}^{\mathrm{II}} + r_{vv}^{\mathrm{II}}) \cdot \mathrm{e}^{\mathrm{j}2k_0 d_0}}. \quad \text{(A16)}$$

If the PCM can realize LTC polarization conversion, it must at least meet the following condition:

$$t_{yy}^{\mathrm{I+II}} = \mathrm{e}^{\pm \mathrm{j}\frac{\pi}{2}} \cdot t_{xy}^{\mathrm{I+II}}. \quad \text{(A17)}$$

Combining with Eqs. (A15) and (A16), the condition can be express as

$$\frac{t_{uu}^{\mathrm{II}}}{t_{vv}^{\mathrm{II}}} = \mathrm{e}^{\pm \mathrm{j}\frac{\pi}{2}} \cdot \frac{(\mathrm{e}^{\mathrm{j}k_0 d_0} + r_{uu}^{\mathrm{II}} \cdot \mathrm{e}^{\mathrm{j}3k_0 d_0})}{(\mathrm{e}^{\mathrm{j}k_0 d_0} + r_{vv}^{\mathrm{II}} \cdot \mathrm{e}^{\mathrm{j}3k_0 d_0})}. \quad \text{(A18)}$$

Substituting Eqs. (A8)–(A11) into Eq. (A18), the condition for achieving LTC polarization conversion based on coefficients of each layer can be derived as follows:

$$\frac{t_{uu}^{\mathrm{B}}}{t_{vv}^{\mathrm{B}}} = \mathrm{e}^{\pm \mathrm{j}\frac{\pi}{2}} \cdot \frac{1 + r_{uu}^{\mathrm{B}} \cdot \mathrm{e}^{\mathrm{j}2k_0 d_0} + r^{\mathrm{C}} \cdot \mathrm{e}^{\mathrm{j}2k_0 d_1} \cdot \{[(t_{uu}^{\mathrm{B}})^2 - (r_{uu}^{\mathrm{B}})^2] \cdot \mathrm{e}^{\mathrm{j}2k_0 d_0} - r_{uu}^{\mathrm{B}}\}}{1 + r_{vv}^{\mathrm{B}} \cdot \mathrm{e}^{\mathrm{j}2k_0 d_0} + r^{\mathrm{C}} \cdot \mathrm{e}^{\mathrm{j}2k_0 d_1} \cdot \{[(t_{vv}^{\mathrm{B}})^2 - (r_{vv}^{\mathrm{B}})^2] \cdot \mathrm{e}^{\mathrm{j}2k_0 d_0} - r_{vv}^{\mathrm{B}}\}}. \quad \text{(A19)}$$

Acknowledgement

Project supported by the Fundamental Research Funds for Central Universities (Grant No. 2682020GF03).

References

[1] Nama L, Nilotpal, Bhattacharyya and Jain P K 2021 *IEEE Antennas Propag. Mag.* **63** 100
[2] Hu Q, Chen K, Zheng Y L, Xu Z Y, W J, Zhao J M and Feng Y J 2021 *J. Radars* **10** 304
[3] Shokati E and Granpayeh N 2020 *J. Nanophoton.* **14** 016015
[4] Yang J J, Liao Z Q, Li Y R, Li D M, Wang Z K, Wang T, Wang X and Gong R Z 2021 *Opt. Mater.* **119** 111374
[5] Pandit S, Mohan A and Ray P 2020 *IEEE Antennas Wirel. Propag. Lett.* **19** 2102
[6] Wu Z X, Zhu J X, Zou Y Y, Deng H, Xiong L, Liu Q C and Shang L P 2021 *Opt. Mater.* **123** 111924
[7] Cui Y, Jiang H, Wang L, Liu B Y, Song J and Jiang Y Y 2020 *Appl. Opt.* **59** 3825
[8] Li W, Xia S, He B, Chen J Z, Shi H Y, Zhang A X, Li Z R and Xu Z 2016 *IEEE Trans. Antennas Propag.* **64** 5281
[9] Ma X L, Pan W B, Huang C, Pu M B, Wang Y Q, Zhao B, Cui H J, Wang C T and Luo X G 2014 *Adv. Opt. Mater.* **2** 945
[10] Li Y, Cao Q S and Wang Y 2018 *IEEE Antennas Wirel. Propag. Lett.* **17** 1314
[11] Chen K, Feng Y J, Cui L, Zhao J M, Jiang T and Zhu B 2017 *Sci. Rep.* **7** 42802
[12] Tian J H, Cao X Y, Gao J, Yang H H, Han J F, Yu H C, Wang S M, Jin R and Li T 2019 *J. Appl. Phys.* **125** 135105
[13] Yang Z Y, Kou N, Yu S X, Long F, Yuan L L, Ding Z and Zhang J P 2021 *IEEE Microw. Wirel. Compon. Lett.* **31** 557
[14] Gao X, Yang W L, Ma H F, Cheng Q, Yu X H and Cui T J 2018 *IEEE Trans. Antennas Propag.* **66** 6086
[15] Yu H C, Cao X Y, Gao J, Yang H H, Jidi L, Han J F and Li T 2018 *Opt. Mater. Express* **8** 3373
[16] Huang C X, Zhang J J, Cheng Q and Cui T J 2021 *Adv. Funct. Mater.* **31** 2103379
[17] Huidobro P A, Kraft M, Maier S A and Pendry J B 2016 *ACS Nano.* **10** 5499
[18] Pawlik G, Tarnowski K, Walasik W, Mitus A C and Khoo I C 2012 *Opt. Lett.* **37** 1847
[19] Cheng Y Z, Nie Y, Cheng Z Z and Gong R Z 2014 *Prog. Electromagn. Res.* **145** 263
[20] Xu H X, Wang G M, Qi M Q and Cai T 2013 *Prog. Electromagn. Res.* **143** 243
[21] Zheng Q, Guo C J, Vandenbosch G A E, Yuan P L and Ding J 2020 *IET Microw. Antennas Propag.* **14** 967
[22] Ni C, Chen M S, Zhang Z X and Wu X L 2018 *IEEE Antennas Wirel. Propag. Lett.* **17** 78
[23] Li L, Li Y J, Wu Z, Huo F F, Zhang Y L and Zhao C S 2015 *Proc. IEEE* **103** 1057
[24] Grady N K, Heyes J E, Chowdhury D R, Zeng Y, Reiten M T, Azad A K, Taylor A J, Dalvit D A R and Chen H T 2013 *Science* **340** 1304
[25] Jing X F, Gui X C, Zhou P W and Hong Z 2018 *J. Lightwave Technol.* **36** 2322
[26] Xu K K, Xiao Z Y, Tang J Y, Liu D J and Wang Z H 2016 *Physica E* **81** 169
[27] Liu K Y, Wang G M, Cai T, Li H P and Li T Y 2021 *IEEE Trans. Antennas Propag.* **69** 3349
[28] Li H, Wang G, Liang J, Gao X, Hou H and Jia X 2017 *IEEE Trans. Antennas Propag.* **65** 1452
[29] Abadi S M A M H and Behdad N 2016 *IEEE Trans. Antennas Propag.* **64** 525
[30] Lin B Q, Lv L T, Guo J X, Wang Z L, Huang S Q and Wang Y W 2020 *Chin. Phys. B* **29** 104205
[31] Zhang F H, Yang G M and Jin Y Q 2020 *IEEE Trans. Antennas Propag.* **68** 6646
[32] Wang H B, Cheng Y J and Chen Z N 2020 *IEEE Trans. Antennas Propag.* **68** 1186